NATIONAL ADVISORY COMMITTEE FOR AERONAUTICS

TECHNICAL NOTE 4327

HYPERSONIC VISCOUS FLOW OVER SLENDER CONES

By Lawrence Talbot, Toyoki Koga and Pauline M. Sherman
University of California

Washington
September 1958

NATIONAL ADVISORY COMMITTEE FOR AERONAUTICS

TECHNICAL NOTE 4327

HYPERSONIC VISCOUS FLOW OVER SLENDER CONES

By Lawrence Talbot, Toyoki Koga, and Pauline M. Sherman

SUMMARY

Viscous self-induced pressures on 3°-semivertex-angle cones were measured over the range $3.7 <$ free-stream Mach number < 5.8 and $0.5 <$ viscous-interaction parameter < 2.3. The data were found to be in good agreement with results obtained by Talbot on 5° cones in the range $3.7 <$ free-stream Mach number < 4.1 and $0.9 <$ viscous-interaction parameter < 3.5. All these data were correlated reasonably well by the viscous-interaction parameter, which is defined as $\bar{\chi}_c = M_c^3\sqrt{C/Re_{x_c}}$, where M_c and Re_{x_c} are the Mach number and Reynolds number based on ideal Taylor-Maccoll flow conditions and C is the Chapman-Rubesin factor.

A new method for calculating self-induced pressures is presented which takes into account the interaction between boundary-layer growth and the inviscid-flow field at the outer edge of the boundary layer. Pressures calculated by this method were only 10 to 20 percent higher than the measured values.

INTRODUCTION

The fluid-dynamic and thermodynamic phenomena associated with flight at hypersonic speeds have been the subject of intensive research in recent years. In this research one problem that has received considerable attention is the problem of the "self-induced-pressure" effect, which is one aspect of a broader class of phenomena that can be described as "viscous-interaction" phenomena.

The self-induced-pressure effect comes about in the following way. At hypersonic speeds the boundary layers which develop on bodies are, because of the large temperature differences generated through them, many times thicker than those which are produced at low speeds. Since the density of the hot gas in a hypersonic boundary layer is very low, the mass flux within the boundary layer is small. Thus, the presence of a thick layer of hot gas adjacent to the surface of a body results in the outward displacement of streamlines in the flow external to the layer;

this outward displacement can be regarded as equivalent to an effective thickening of the body (see fig. 1). It can easily be seen that this thickening will result in increases in pressure in the flow external to the boundary layer, and because the pressure in the external flow is transmitted essentially without change through the boundary layer, the pressures on the surface of the body will likewise be increased. The difference between the actual surface pressure and that calculated by inviscid theory neglecting the boundary layer is called the self-induced pressure.

Although the fundamental mechanism responsible for self-induced pressures is well understood, the analysis of the effect is rather complicated. The magnitude of the self-induced pressure is directly proportional to the rate of growth of the boundary layer. However, the growth of the boundary layer is determined by the pressure, Mach number, and so forth in the flow at the outer edge of the layer, and the values of these quantities depend on the magnitude of the displacement effect. It is seen, therefore, that the problem under consideration is a complex interaction phenomenon in which the boundary-layer history plays an important role. It will also be recognized that the magnitude of the phenomenon is more significant for thin bodies such as flat plates and slender cones than for thick bodies, since for thin bodies the changes in effective geometry due to boundary-layer growth will be proportionately larger.

The particular problem considered in this report is the effect of self-induced pressure on a slender cone. In the first part of the report new data are presented for pressures on 3° semivertex angle cones. The two appendixes discuss several of the analyses which have been proposed for predicting the effect and present a new method of calculating self-induced pressures.

This investigation was carried out at the University of California under the sponsorship and with the financial assistance of the National Advisory Committee for Aeronautics.

SYMBOLS

C Chapman-Rubesin factor in relation $(\mu/\mu_2) = C(T/T_2)$

d diameter of pressure orifice

K_c similarity parameter, $M_1\theta_c$

K_2 similarity parameter, $M_1\theta_2$

M Mach number

p static pressure

Re Reynolds number

r radial distance measured outward from cone axis

r_c cone radius

T gas temperature

t bluntness of cone tip or thickness of leading edge of plate

u gas velocity

x distance measured from vertex along cone surface

y distance normal to cone surface

γ ratio of specific heats

δ boundary-layer thickness

δ^* boundary-layer displacement thickness, $\int_0^\infty \left[1 - (\rho u/\rho_2 u_2)\right] dy$

δ_1^* displacement thickness on cone, corrected for transverse curvature

θ_c cone semivertex angle

θ_δ streamline inclination at outer edge of boundary layer, $\tan^{-1}\left(\frac{d\delta^*}{dx}\right)$

θ_2 $\theta_c + \theta_\delta$

Λ mean free path

μ absolute viscosity

ν kinematic viscosity

ρ gas density

σ Prandtl number

$\overline{\chi}_c$ viscous-interaction parameter, $M_c^3\sqrt{C/Re_{x_c}}$

Subscripts:

aw adiabatic wall

c ideal flow conditions along surface of cone obtained for $x \to \infty$

w wall conditions

Λ property evaluated at distance Λ from wall

1 free-stream conditions

2 conditions at outer edge of cone boundary layer, taken to be functions of x

Examples of the notation used for the various Reynolds numbers are:
$Re_2/inch = u_2/\nu_2$, $Re_{t_1} = u_1 t/\nu_1$, and $Re_{x_c} = u_c x/\nu_c$

PREVIOUS EXPERIMENTAL RESULTS

The only data which have been available up to now for viscous interacting flow over a cone seem to be from the experiments of Talbot and Baldwin (refs. 1 and 2, respectively). Talbot obtained his data in the Low-Density Wind Tunnel of the University of California. His tests were carried out on 5°-semivertex-angle cones, in the Mach number range $3.7 < M_1 < 4.1$, and at Reynolds numbers which corresponded to the viscous-interaction-parameter range $0.9 < \bar{\chi}_c < 3.5$. Baldwin obtained data at the Guggenheim Aeronautical Laboratory, California Institute of Technology, in the 5- by 5-inch hypersonic wind tunnel, leg number 1. His data were also for a 5° cone, at $M_1 = 5.8$, and $0.1 < \bar{\chi}_c < 1.6$.

APPARATUS

Wind Tunnel

The experiments for the present work were conducted in the No. 4 Low Density Wind Tunnel of the University of California. This wind tunnel, which is an open-jet continuous-flow type employing axially symmetric nozzles, has been described in detail in several publications (refs. 1, 3, 4, and 5). Two nozzles were used in the tests: the No. 8 nozzle, which produces flows in the range $3.7 < M_1 < 4.1$, $900 < Re_1/inch < 3,600$; and the No. 9 nozzle, which produces flows in the range $5.5 < M_1 < 5.8$, $4,000 < Re_1/inch < 9,000$. Actual values of the flow parameters obtained in the tests are listed in table I.

Models

All the cones tested were of 3° semivertex angle. Two sets of models were used, each set consisting of seven cones. The type A cones had base diameters of 0.500 inch, and the type B cones had base diameters of 0.750.inch. The longer type B models were designed primarily to investigate the influence on the cone surface pressure of the expansion

wave generated at the juncture of the conical surface and the cylindrical afterbody.

Each cone had four 0.010-inch-diameter pressure orifices spaced circumferentially at 90° intervals at a prescribed distance from its vertex. The vertex distances are listed in figure 2. Also shown in this figure is the collar and set screw arrangement at the base of the cross-stream supports of the models which was used to aline them parallel to the axis of the wind-tunnel nozzle. Figure 3 shows the type A models, together with an impact probe, mounted on the rotary probe selector of the traverse mechanism.

Subsequent to its use in the pressure measurement tests, model B7 was fitted with four copper-constantan thermocouples soldered in the cone surface at 2, 3, 4, and 5 inches from the vertex. This model provided information on the wall temperature of the cones, which was required for the boundary-layer calculations.

Some difficulty was encountered in producing models with sharp tips. The method of fabrication which was found most satisfactory was an acid etching process. After the cones had been machined, the tip regions were etched by a flat tool covered with a thin film of nitric acid. This method produced tips with diameters less than 0.001 inch. However, the etching was not completely uniform. In the etched regions of the models, which extended back from the vertices about 0.4 inch, some local variations in cone angle of several degrees were observed. Farther back from the vertices all cone angles were found to be $3.03^{\circ} \pm 0.03^{\circ}$.

Instrumentation

Cone surface pressures were measured with the temperature-regulated thermistor manometer described in reference 3. This instrument was used because of its small gage volume and short tubulation, which results in a fast time response, and because of its high accuracy in the measurement of the difference between nearly equal pressures. The thermistor is mounted on the traverse mechanism of the wind tunnel, and pressures within the models are led to it through a valve mechanism on the rotary probe selector. The least count (0.1 mv) of the potentiometer used to measure the bridge unbalance of the thermistor measuring circuit corresponded to a pressure increment of about 0.02 micron of mercury. Before each test the thermistor was calibrated statically against a precision McLeod gage (ref. 6). Analysis of the thermistor calibration data yielded a probable error in absolute pressure of about 1 percent. It took about 1 minute for the cone-thermistor system to come to equilibrium after a change in pressure was imposed on a model by placing it in the flow.

Wind-tunnel stagnation pressures were measured with a mercury manometer. Impact pressures were measured with a butyl phthalate oil manometer (ref. 7). Both manometers are equipped with magnifying optics which make it possible to locate the menisci to within 0.001 inch.

Nozzle Calibration

Mach numbers and static pressures in the test regions of the nozzles were determined by measuring stagnation and impact pressures, assuming the flow to be isentropic. For each flow condition of the tests an axial impact-pressure survey was made to determine the Mach number and static-pressure variations in the regions occupied by the models.

The impact-pressure surveys in the No. 8 nozzle revealed a region about 8 inches in axial extent over which the Mach number variation was less than 2 percent and the static-pressure variation less than 10 percent. In the No. 9 nozzle the axial extent of the region over which the Mach number and static-pressure variations were less than these values was about 3.5 inches.

TEST PROCEDURE

The test models and an impact probe were mounted on the rotary probe selector of the traverse mechanism and allowed to outgas under vacuum for 2 days. At the beginning of a test the flow was established and measured by means of the impact tube, under "balanced-jet" conditions, which required that the pressure measured on the wall of the nozzle be equal to the static pressure in the chamber surrounding the open jet. (This balance condition did not alter appreciably when the models replaced the impact tube in the stream.)

After flow was established, the test models were successively rotated into the stream, and cone surface pressures were measured. Before a measurement was made, sufficient time (about 10 to 15 min.) was allowed to permit the model to come to thermal equilibrium; during this period the cone pressure decreased slowly because the cooling of the model caused a thinning of the boundary layer.

In the tests reported, all models were positioned so that their vertices were located at the same point in the flow. Correction was made for the axial gradients. Other tests were made with models positioned so that their respective pressure orifices were at the same axial location in the stream. The surface pressures obtained by this second method agreed quite well with those obtained by the first method. In the first method the correction for axial gradients in the stream was

accomplished simply by using the local Mach numbers obtained from the impact-pressure surveys to determine values of the inviscid surface pressure p_c corresponding to the actual location of the pressure orifices. These values were used with the measured cone pressures p_2 to obtain the ratio p_2/p_c.

It was found that the above correction procedure gave consistent results provided the static pressure in the flow at the point where orifices were located did not differ by more than 10 percent from that at the vertex of the model. Consequently, in the No. 9 nozzle, where the axial extent of usable flow was about 3.5 inches, only models B1, B2, and B3 were used for the final tests. No difficulties arose on this score in the No. 8 nozzle. However, it was observed that the expansion-wave reflection of the bow shock (the reflection occurring in the region of the strong density gradient where the isentropic core merged with the nozzle boundary layer) affected the pressures measured on models B6 and B7. For this reason data are not reported at $M \approx 4$ for these models.

The temperature measurements made with model B7 showed the surface of the cone to be isothermal. The apparent recovery factor (based on inviscid-flow conditions M_c and T_c behind the conical shock) was about 0.89; the increase over the theoretical value of 0.85 for the laminar boundary layer is due to heat conduction through the support from the model mounting, which was at essentially stagnation temperature.

RESULTS

Results of the tests are given in terms of the induced-pressure increment $(p_2/p_c) - 1$. The inviscid-flow pressures for the 3° cones were calculated from Van Dyke's second-order theory (ref. 8), since interpolation in the Kopal tables (ref. 9) between 0° and 5° was not sufficiently accurate. The data at different flow conditions are shown plotted against x in figure 4, and in figure 5 against the viscous-interaction parameter $\overline{\chi}_c = M_c^3\sqrt{C/Re_{x_c}}$, where M_c and Re_{x_c} are the Mach number and Reynolds number based on ideal Taylor-Maccoll flow conditions.

Numerical values for the induced-pressure increment are in the range 0.06 to 0.30. The actual measured cone pressures varied between about 60 and 170 microns of mercury. An error of 1 percent in the measured pressure is equivalent to an error in the induced-pressure increment of 5 percent or more for most of the data, assuming the values of p_c to be exact, and from this it is estimated that the over-all probable errors in $(p_2/p_c) - 1$ are between 5 and 15 percent. Free-stream Mach numbers are accurate to about 1 percent; free-stream Reynolds numbers are accurate to about 5 percent.

In addition to the results of the present tests, two sets of data taken from reference 1 are shown in figure 6. In figure 5 all the reference 1 data for 5° models A1 through A7 are plotted. The data from reference 2, which are also for 5° cones, are represented by a single line in figure 5.

DISCUSSION

Experimental Results

One conclusion which can be drawn from an examination of figure 4 is that the effect of the shoulder expansion did not extend far enough upstream in the cone boundary layer to influence the cone surface pressures. This is evidenced by the fact that the data obtained with the B models agree, within experimental scatter, with those obtained with the A models. It was not possible to determine the extent of the region on the cone which is influenced by the shoulder expansion, because the reflection of the bow shock wave back onto the models obscured the effect. Models B6 and B7, which were designed to measure the upstream influence, were those most affected by the reflected wave. In figure 4 it can be noted that the pressure orifice on model B5 was also within the zone influenced by the reflection.

The scatter in the data is probably due to a combination of experimental error, imperfections in the orifices, and inaccuracies in the cone angle in the tip regions of the models. One may note that the reproducibility of the data was quite good, as evidenced by the comparisons shown in figures 4(e) and 4(f) between different sets of measurements made with both the A and the B models.

It can be seen from figure 5 that the parameter $\overline{\chi}_c$ provides a fairly good correlation for all the data obtained in the University of California Low Density Wind Tunnel. The Mach 4 data for the 3° and 5° cones agree quite well; the Mach 5.6 data are slightly lower.

It can also be seen from figure 5 that the induced-pressure increments of reference 2 are higher, by a factor of about 2, than those obtained here. One suggestion which has been advanced is that the differences may be due in part to the influence of tip bluntness. It is true that the Reynolds numbers based on tip diameter were higher in experiments of reference 2 than in the present one. The former were mostly in the range $65 < Re_{t_1} < 230$, whereas all the data from the Low Density Wind Tunnel correspond to $Re_{t_1} < 9$. However, it seems unlikely that tip bluntness could account for much of the difference. The experiments on flat plates (refs. 10 and 11) indicate that below about $Re_{t_1} = 80$ the plate can be considered as sharp, and the effect of tip bluntness has been shown to be much less pronounced for cones than for flat plates (ref. 12).

Comparisons Between Theory and Experiment

Three methods for calculating self-induced pressures have been employed in this report. The first, a new method devised by the present authors and called the TC method, is presented and discussed in appendix A. The second, a method proposed by Probstein, is reviewed and commented on in appendix B, as is the third, which herein is called the TC_∞ method. Since the differences between the three methods are discussed in the appendixes, only the comparisons between theory and experiment are noted here.

It can be seen in figures 4 and 6 that the new method for calculating self-induced pressures generally overestimates by about 10 to 20 percent the data obtained in the low-density wind tunnel. In contrast, the TC_∞ method and the Probstein method using two terms in the series both give values greater by a factor of about 2 than the experimental results. The better agreement obtained with the present method is not surprising; of the three methods it is the only one which accounts in even an approximate way for the true interaction effect, wherein the changes in the external flow due to the presence of the boundary layer feed back into the layer and alter its rate of growth.

It may be remarked that the present theory has also been compared with recent measurments of self-induced pressures on flat plates (ref. 10). The agreement was found to be quite good. The term in the expression for θ_δ involving the derivative dM_2/dx (see appendix A) is not negligible in the flat-plate case. When it is included, the calculated values of p_2/p_1 are increased by nearly 20 percent in the region near the leading edge. The effect of this term was of the order of 5 percent at most for the present case, and it was neglected.

In figure 5, the results of the present theory are represented by a single straight line, and the good agreement between the present theory and the low-density-wind-tunnel data is clearly evident. (Actually, the individual curves of figs. 4 and 6 when plotted against $\bar{\chi}_c$ deviated about ± 2 to 4 percent from this mean line, but were very nearly linear. The deviations do not seem to follow any particular trend and are most probably the result of inaccuracies which were introduced in the graphical parts of the analysis.)

One rather interesting feature of the data is that they appear to be quite linear in $\bar{\chi}_c$. Also, the present method gives theoretical curves which are much more nearly linear than either of the two other methods. It may be that the interaction effect results in a boundary-layer growth which by coincidence gives induced pressures which are almost linear in $\bar{\chi}_c$, at least for $\bar{\chi}_c < 4$.

Hole-Size Effect

It has been shown by Talbot (ref. 1), Rayle (ref. 11), and others that the apparent pressure sensed by a static-pressure orifice increases with the diameter of the orifice. The phenomenon is due to mixing between the stream passing over the surface and the fluid confined within the orifice and pressure tubulation. The momentum transferred by the mixing sets up currents in the fluid within the orifice which give rise to the increase in pressure.

Ideally, a static-pressure orifice should be as small in diameter as possible, both to minimize this hole-size effect and to provide a truly localized pressure measurement. However, in rarefied gas flow if a pressure orifice is made small enough one encounters another effect known as thermal transpiration which can also result in errors in pressure measurement. The thermal-transpiration effect occurs, for example, when an orifice whose diameter is small compared with the mean free path in the gas separates two regions of gas at different temperatures (ref. 14). It is easily shown that in this case the pressure ratio is given by

$$\frac{p_1}{p_2} = \sqrt{\frac{T_1}{T_2}} \tag{1}$$

The static-pressure orifices used in the present experiments were 0.010 inch in diameter. For an orifice of this size, the pressure increment due to momentum mixing is completely negligible. However, there is the possibility that thermal-transpiration effects may be important, since the boundary layer is a region of strong temperature gradient, and many of the molecules which enter the orifice from the gas stream come from regions in the boundary layer which are at temperatures different from the gas within the orifice.

A rough estimate of the magnitude of the thermal-transpiration effect can be made in the following way. Assume the boundary-layer characteristics to be given with sufficient accuracy by Howarth's analysis (ref. 15). For an insulated cone, with $\sigma = 1$ and $\mu/\mu_2 = T/T_2$,

$$\delta \approx \frac{5.0}{\sqrt{3}} \left(1 + 0.08\, M_2^2\right) \sqrt{\frac{\nu_2 x}{u_2}} \tag{2}$$

$$\frac{T}{T_{aw}} = \frac{1 + 0.2\, M_2^2 \left[1 - \left(u^2/u_2^2\right)\right]}{1 + 0.2\, M_2^2} \tag{3}$$

Now, also assume that the velocity distribution in the boundary layer is linear in y. Then the temperature T_Λ at a distance Λ_w from the wall is given by

$$\frac{T_\Lambda}{T_{aw}} = \frac{1 + 0.2\, M_2^2(1 - \Lambda_w^2/\delta^2)}{1 + 0.2\, M_2^2} \tag{4}$$

where Λ_w is the mean free path of the gas at the wall.

As a specific example, take the following conditions: $M_2 = 5.5$; $Re_2 = 10{,}000/\text{inch}$; $p_2 = 170$ microns of mercury; $x = 1$ inch; and $T_{aw} = 270^\circ$ K. For these conditions $\Lambda_w \approx 0.011$ inch and $\delta \approx 0.099$ inch. Then from equation (1), $p_\Lambda/p_w = 0.994$, where p_Λ is the pressure in the boundary layer and p_w is the pressure within the orifice, which is presumably different from p_Λ because of the thermal-transpiration effect. It is seen that for this particular case the error is about 1/2 percent. For the worst conditions encountered in the tests, the error is about 2 percent. Actually, this analysis greatly overestimates the effect, since equation (1) is true only for $\Lambda_w/d \gg 1$. For the experiments $\Lambda_w/d \approx 1$, and in this range the pressure increment is less than 10 percent of what it is in free molecule flow. One may conclude, therefore, that the pressures measured in the experiments were true static pressures, essentially uninfluenced by either momentum mixing or thermal-transpiration hole-size effects.

CONCLUSIONS

The results of the investigation of viscous self-induced pressures on 3°-semivertex-angle cones may be summarized as follows:

1. The new data obtained for self-induced pressures on 3° cones are in good agreement with previous data obtained on 5° cones. All these data are correlated reasonably well by the hypersonic-viscous-interaction parameter $\overline{\chi}_c = M_c^3\sqrt{C/Re_{x_c}}$, where M_c and Re_{x_c} are Mach number and Reynolds number based on ideal Taylor-Maccoll flow conditions and C is the Chapman-Rubesin factor.

2. The tangent-cone viscous-interaction model predicts self-induced pressures which are only 10 to 20 percent higher than the measured values, if local values of the flow parameters at the edge of the boundary layer are used in calculating the boundary-layer growth.

University of California,
Berkeley, Calif., June 24, 1957.

APPENDIX A

NUMERICAL-GRAPHICAL METHOD FOR CALCULATING SELF-INDUCED PRESSURES ON CONE SURFACE

The self-induced pressure generated on the surface of a cone in hypersonic flow because of the outward displacement of the external flow streamlines by boundary-layer growth has been studied by several authors (refs. 16 and 17). The assumptions usually made are: (1) A region of inviscid flow exists between the outer edge of the boundary layer and the shock wave, and (2) the flow parameters, such as Mach number or pressure, at the edge of the boundary layer (subscript 2 in fig. 1) can be obtained to satisfy approximations by the tangent-cone (TC) method. The tangent-cone method consists of relating the local flow parameters on a body to the undisturbed flow ahead of the shock wave through conical-flow theory (e.g., Taylor-Maccoll values), but using the local body inclination as the effective cone angle. In the case of self-induced pressures on a cone as shown in figure 1, the local effective cone angle is taken to be θ_2, the sum of the cone angle θ_c and the angle $\theta_\delta = \tan^{-1}\left(\frac{d\delta^*}{dx}\right)$.

Two computations are involved in utilizing the TC method for evaluation of self-induced pressures. First, the inviscid-flow values must be obtained, for given effective cone angle θ_2, either from the exact solution (Kopal's tables) or by one of several approximate methods (refs. 18 and 19) which are available. Secondly, the boundary-layer displacement thickness must be evaluated as a function of position along the cone surface, and here again several methods of varying accuracy and complexity are available. It will be noticed that the two computations are not independent, since the boundary-layer growth determines the inviscid-flow values at the outer edge of the boundary layer, but at the same time the rate of growth of the boundary layer is determined by these inviscid-flow values. An accurate application of the TC method must include this interaction effect.

For the computations of the inviscid-flow values, it was decided to use the exact Taylor-Maccoll results as computed by Kopal. There are several supersonic and hypersonic flow approximations in analytic form which are accurate over different ranges of the similarity parameter $K_2 = M_1\theta_2$, but no single one is sufficiently accurate over the entire range of K_2 encountered in the tests reported here.

For the computation of the growth of boundary-layer displacement thickness $d\delta^*/dx$, it would be desirable to have a method which takes into account the external-flow pressure gradient, the transverse-

curvature effect, an accurate viscosity-temperature relation, the appropriate value for the Prandtl number, and the actual measured wall temperature. The formula for δ^* which is used here, and taken from reference 20, fulfills all the foregoing requirements with the exception of the consideration of the external-flow pressure gradient and transverse-curvature effect. The approximate expression of reference 20 employs the Chapman-Rubesin factor C evaluated in a way which gives close agreement with Crocco's exact calculation based on the Sutherland law. The effect of isothermal wall temperature different from the adiabatic value and the effect of Prandtl number are also included, but the results are valid only for zero pressure gradient. To account in some measure for the effect on the boundary layer of the variation in the external-flow quantities along its outer edge, local values of the external-flow parameters are used to calculate M_2 and Re_{x_2}. This method does not take into account changes in the velocity, temperature, and density distributions within the boundary layer caused by the external-flow gradients.

Method of Computation

The computation method employed is a semigraphical one.

Inviscid flow; TC approximation. - For a given free-stream condition (M_1, p_1, T_1, and Re_1), plots of M_2, p_2/p_1, T_2/T_1, and Re_2 are constructed as functions of equivalent effective cone angle θ_2. Interpolation in Kopal's tables and the adiabatic law are used to obtain these values. Viscosities are taken directly from a plot of the semi-empirical formula of reference 21. Curves of the form shown in sketches (a) and (b) are obtained.

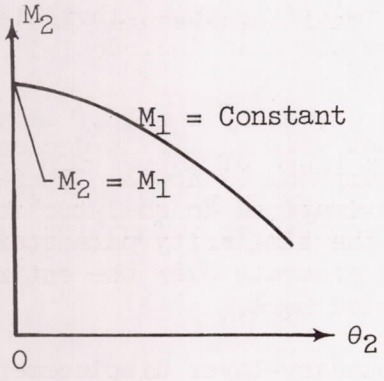

(a)

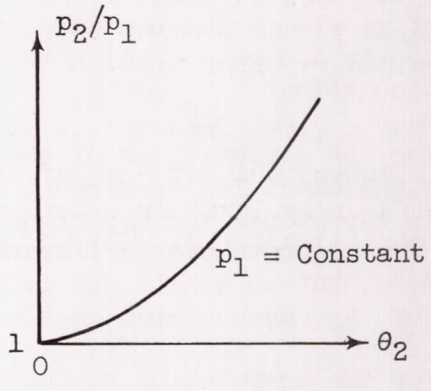

(b)

Boundary-layer displacement thickness. - The approximate result of reference 20, to which the Mangler transformation correction $1/\sqrt{3}$ (ref. 22) has been applied, is

$$\left.\begin{aligned}\frac{\delta^*}{x} &= \sqrt{\frac{C}{Re_{x_2}}}\left\{\frac{\pi}{2}\left(\frac{T_w}{T_2} - \frac{\sigma(\gamma - 1)}{4}M_2^2\right) - \left[1 + \sigma^{1/3}\left(\frac{T_w}{T_2} - \frac{T_{aw}}{T_2}\right)\right]\right\} \\ \frac{d\delta^*}{dx} &\approx \frac{1}{2}\sqrt{\frac{C}{Re_{x_2}}}\left\{\pi\left(\frac{T_w}{T_2} - \frac{\sigma(\gamma - 1)}{4}M_2^2\right) - \left[1 + \sigma^{1/3}\left(\frac{T_w}{T_2} - \frac{T_{aw}}{T_2}\right)\right]\right\}\end{aligned}\right\} \quad (A1)$$

where

$$\frac{T_{aw}}{T_2} = 1 + \sigma^{1/2}\frac{(\gamma - 1)}{2}M_2^2 \quad (A2)$$

and the Chapman-Rubesin factor C is defined by

$$C = \frac{\mu'/\mu_c}{T'/T_c} \quad (A3)$$

The viscosity μ' is evaluated at the intermediate temperature T' given by

$$T'/T_c = (T_w/T_c) - 0.468\,\sigma^{1/3}\left[(T_w/T_c) - (T_{aw}/T_c)\right] - 0.273\,\sigma\frac{(\gamma - 1)}{2}M_c^2 \quad (A4)$$

However, instead of using the Sutherland law, as recommended in reference 20, the values of reference 21 are used for μ'/μ_c, since the Sutherland law is less accurate at the low free-stream temperatures encountered in the present tests. The actual wall temperature T_w is determined by experiment.

For a given free-stream condition (M_1, p_1, etc.) a set of values of θ_2 is chosen and for each of these values a range of values of θ_δ is computed using local free-stream conditions given by plots similar to sketches (a) and (b). The angle θ_δ is presented as a function of x

for each selected value of θ_2 and may be represented graphically as shown in sketch (c).

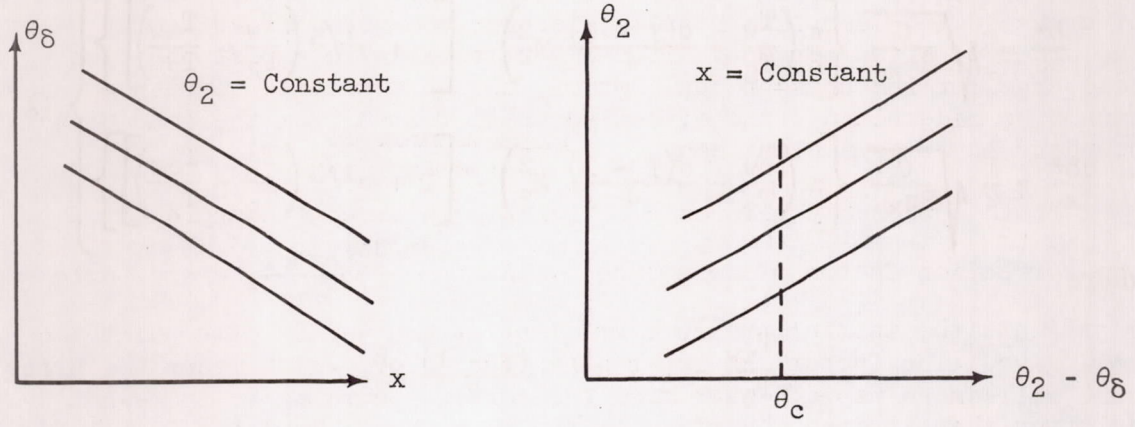

(c) (d)

The value of x appropriate to a particular value of θ_2 is that for which $\theta_2 - \theta_\delta = \theta_c$, the cone angle. Thus, the values displayed in sketch (c) are replotted with x as a parameter in the form shown in sketch (d). The particular values of $\theta_2(x)$ for which $\theta_2 - \theta_\delta = \theta_c$ are then used in connection with sketch (b) to obtain p_2/p_1 as a function of x, where p_2/p_1 is the cone free-stream pressure ratio, including the self-induced pressure. The ideal Taylor-Maccoll pressure ratio p_c/p_1, corresponding to $\theta_2 = \theta_c$, can of course be obtained directly from sketch (b), or in the case of the 3° cones, from Van Dyke's second-order theory.

Discussion

Accuracy of TC method for calculating inviscid flow. - The TC method has been utilized in its most accurate form, namely, with exact values taken from the Kopal tables. This was necessary because neither the hypersonic approximation of reference 18 nor the Kármán-Moore slender-body result (ref. 23) is sufficiently accurate for K_2 of the order of unity, which is the range encountered in the present tests. However, it must be remembered that the TC method itself provides only an approximation to the inviscid-flow field. The accuracy of the method has been examined (refs. 17 and 24) by comparing results obtained by it for pressure

distributions on pointed ogives with exact values obtained from the method of characteristics. The TC method yields surface pressures which are slightly higher than the exact values, the difference depending on the distance from the vertex of the ogive. At the vertex the two methods, of course, give identical results; farther back the deviation may be of the order of a few percent. It seems reasonable to expect the same to hold true for the present application, though a precise correspondence cannot be made because the effective shape formed from the cone plus the boundary layer is a blunt body.

It is noted that reference 2 gives an incorrect interpretation to the correction factor of reference 17 $\lambda = \frac{(dp/ds)_{exact}}{(dp/ds)_{TC}}$, where dp/ds represents the initial pressure gradient at the vertex of a pointed convex ogive. The factor λ is greater than unity, which means the pressure falls more rapidly back from the vertex according to the exact calculation than it does according to the TC method. Thus the TC method overestimates the pressure. In reference 2 the factor is written incorrectly as $\lambda = \frac{(dp/d\theta)_{exact}}{(dp/d\theta)_{TC}}$ and from this it is inferred that the method underestimates the pressure.

Induced-pressure flow model. - The basic idea used in the TC calculation for self-induced pressures is that the effect of boundary-layer growth on the external inviscid flow can be evaluated approximately by increasing the effective local cone angle by the amount $\theta_\delta = \tan^{-1}(d\delta^*/dx)$. Order-of-magnitude arguments concerning the accuracy of this approximation are given in references 11, 16, and 17. The error involved in replacing the actual streamline inclination in the external flow by the slope θ_δ is estimated to be of the order $(\delta/x)^2$, where δ is the boundary-layer thickness. It also turns out that the neglect of pressure gradient across the boundary layer is justified provided $(\delta/x)^2$ is small.

Boundary-layer calculations. - The boundary-layer calculations used in this report account in some measure for the variation in external-flow properties along the outer edge of the boundary layer by using local values for M_2, Re_2, p_2, and so forth. However, the expression for $d\delta^*/dx$ (eq. (A1)) is only approximate, since the terms involving dM_2/dx, dT_2/dx, and dRe_2/dx have been neglected. It turns out that for the present calculations these terms contribute an increment of about 5 percent at the most to θ_δ, and their neglect is not serious.

Two effects which have not been accounted for in the boundary-layer analysis are the effect of transverse curvature and the direct effect of the self-induced pressure gradient on the density and velocity distribu-

tions within the boundary layer. Both the transverse curvature and the pressure gradient tend to thin the boundary layer and thus result in smaller values for the induced-pressure increment. The transverse-curvature effect has been studied by Probstein and Elliott (ref. 25). Probstein concludes (ref. 26) from his analysis, which is valid for small δ^*/r_c, that transverse curvature does not appreciably alter the boundary-layer displacement thickness. However, much of the present data were in the range $\delta^*/r_c = 1 - 3$, and for these values the transverse-curvature effect almost certainly cannot be neglected.

In reference 27 a correction for transverse curvature is deduced which gives $\frac{d\delta_1^*}{dx} = \frac{d\delta^*/dx}{\sqrt{1 + 2\delta^*/r_c}}$, where δ_1^* is the displacement thickness, including transverse curvature, and δ^* is the displacement thickness on the cone in the absence of curvature effects (i.e., eq. (A1) of this report). This result is based on the assumption, suggested by the calculations of reference 24, that the integral $\int_{r_c}^{\infty}\left(1 - \frac{\rho u}{\rho_2 u_2}\right)\frac{r\,dr}{r_c} = \delta_1^*$ is unaffected by transverse curvature. Then the identification $\delta_1^* = \int_{r_c}^{r_c+\delta^*} \frac{r}{r_c}\,dr$ is made, and the result for $\frac{d\delta_1^*}{dx}$ cited above follows immediately. If one applies this transverse curvature correction to the present data it is seen that for $\frac{\delta^*}{r_c} \approx 1$ (roughly the lower limit of the data) the result cited above predicts a decrease in induced pressure of about 40 percent, while for the largest value, $\frac{\delta^*}{r_c} \approx 3$, the decrease is about 60 percent. These decrements in pressure seem much too large, and it is probable that the assumptions used to obtain $\frac{d\delta_1^*}{dx}$ are not good approximations for values of $\frac{\delta^*}{r_c}$ as large as those of the present tests.

Evaluation of results of calculations. - It can be seen from figures 4(f) and 6 that the method given in this appendix yields induced-pressure increments which are smaller by factors of about 1.5 to 1.8 than those obtained from the Probstein and TC methods. The difference is due solely to the interaction process, which has been approximated by using local values for M_2, Re_2, p_2, and so forth in the calculation of $d\delta^*/dx$.

An improvement in the accuracy of the present method could probably be made by accounting for some of the neglected effects which have been mentioned in the foregoing discussion. For example, the calculated induced pressure would be increased by (1) including the gradient terms

dM_2/dx, and so forth, in the expression for $d\delta^*/dx$, and (2) correcting for the error involved in the approximation $\theta_\delta = \tan^{-1}(d\delta^*/dx)$. On the other hand, the calculated induced pressures would be decreased by: (1) including the transverse-curvature effect, (2) correcting for the error in the TC approximation for the inviscid-flow field, (3) including the pressure gradient across the boundary layer, and (4) including the direct effect on boundary-layer growth of the pressure gradient along the outer edge of the boundary layer.

APPENDIX B

PROBSTEIN'S ANALYSIS FOR SELF-INDUCED-PRESSURE EFFECT

Probstein (ref. 26) considers a Taylor series expansion of the surface pressure in the form

$$p_2 = p_c + \left(\frac{\partial p_c}{\partial \theta}\right)_{\theta=\theta_c} \theta_\delta + \frac{1}{2!}\left(\frac{\partial^2 p_c}{\partial \theta^2}\right)_{\theta=\theta_c} \theta_\delta^2 + \cdots \tag{B1}$$

or

$$\frac{p_2 - p_c}{p_c} = \frac{p_1}{p_c}\left\{\left[\frac{\partial (p_c/p_1)}{\partial \theta}\right]_{\theta=\theta_c} \theta_\delta + \frac{1}{2!}\left[\frac{\partial^2 (p_c/p_1)}{\partial \theta^2}\right]_{\theta=\theta_c} \theta_\delta^2 + \cdots\right\} \tag{B2}$$

Now, for $K_c < 1$, which is the range encountered in the present tests, the Lees hypersonic approximation is not accurate, so that the values for the derivatives in equation (B2) obtained by Probstein cannot be used. Probstein suggests that for $K_c < 1$ the ratio p_1/p_c be evaluated from the Kopal tables, but that the derivatives be evaluated from the Kármán slender-body result (ref. 23). However, this result is also not sufficiently accurate. Following Van Dyke's suggestions (ref. 28) for combined supersonic-hypersonic similarity, a formula of the form

$$\frac{p_c}{p_1} = 1 + \frac{A_1 \gamma M_1^2 \theta_c^2}{2} \log_e \left(\frac{A_2}{\theta_c \sqrt{M_1^2 - 1}}\right) \tag{B3}$$

was used to fit the Kopal values and the Van Dyke second-order-theory values for p_c/p_1 over the range $0.14 < \theta_c\sqrt{M_1^2 - 1} < 0.3$, $0 < \theta_c < 0.13$ radian. The constants found were $A_1 = 1.52$ and $A_2 = 2.85$. Expression (B3) was used to calculate the derivatives in equation (B2), and expression (A1) was used to evaluate θ_δ and θ_δ^2, except that inviscid-flow values M_c, Re_c, and T_c were used instead of the local values M_2, Re_2, and T_2.

It was necessary to include at least two terms in the series. For example, with $M_1 = 3.70$, $\theta_c = 5^\circ$,

$$\left.\begin{aligned} \frac{p_1}{p_c}\left[\frac{\partial(p_c/p_1)}{\partial\theta}\right]_{\theta=\theta_c} &= 3.5 \\ \frac{p_1}{p_c}\left[\frac{\partial^2(p_c/p_1)}{\partial\theta^2}\right]_{\theta=\theta_c} &= 17 \end{aligned}\right\} \tag{B4}$$

As a check on the above values, a numerical differentiation was performed on a curve constructed from cross plots of the Kopal entries and the 3° values calculated by second-order theory, and the values 3.8 and 38 were obtained for the derivatives. The first of these values may be more accurate than that given in equations (B4). Not much accuracy can be claimed for either set, however.

The results of the Probstein analysis are shown in figures 4(f) and 6. The first-order curves were obtained using only the first term in the series (B2), second-order curves using two terms. It can be seen that for small-angle cones (i.e., small K_c) the convergence of the series is slow. This slow convergence is already evident at $K_c = 1$, as can be seen from examination of the functions presented in reference 26.

As a check on the Probstein analysis, two induced-pressure distributions were evaluated by what is called here the TC_∞ method. In this method the boundary-layer slope θ_δ is evaluated as above, using inviscid-flow values of T_c, M_c, and Re_c (i.e., the values which obtain far downstream in the flow field external to the boundary layer), and is added point by point to θ_c to obtain θ_2 as a function of x. The pressure distribution p_2/p_1 is obtained directly from a plot of the Kopal entries.

The TC_∞ method of course gives the values that the Probstein method should converge to. As is evident in figures 4(f) and 6, the use of two terms in the Probstein series provides a fairly good approximation. But the method of Probstein is not very useful for $K_c < 1$ because of the difficulty in determining the necessary derivatives with any accuracy.

REFERENCES

1. Talbot, L.: Viscosity Corrections to Cone Probes in Rarefied Supersonic Flow at Nominal Mach Number of 4. NACA TN 3219, 1954.

2. Baldwin, Lawrence C.: Viscous Effects on Static Pressure Distribution for a Slender Cone at a Nominal Mach Number of 5.8. Memo. No. 28, GALCIT, June 14, 1955. (Contract DA-04-495-ORD-19.)

3. Kavanau, L. L.: Base Pressure Studies in Rarefied Supersonic Flows. Jour. Aero. Sci., vol. 23, no. 3, Mar. 1956.

4. Maslach, G. J., and Sherman, F. S.: Design and Testing of an Axisymmetric Hypersonic Nozzle for a Low Density Wind Tunnel. TR 56-341, Univ. Calif., Aug. 1956. (Contract AF-33(616)-418.)

5. Tellep, D. M., and Talbot, L.: Normal Forces on Flat Plates in Low Density Supersonic Flow. Jour. Aero. Sci., vol. 23, no. 12, Dec. 1956.

6. Sherman, F. S.: New Experiments on Impact-Pressure Interpretation in Subsonic and Supersonic Rarefied Air Streams. NACA TN 2995, 1953.

7. Maslach, G. J.: A Precision Differential Manometer. Rev. Sci. Instr., vol. 23, no. 7, July 1952, pp. 367-369.

8. Van Dyke, Milton D.: Practical Calculation of Second-Order Supersonic Flow Past Nonlifting Bodies of Revolution. NACA TN 2744, 1952.

9. Howarth, L.: Concerning the Effect of Compressibility on Laminar Boundary Layers and Their Separation. Proc. Roy. Soc. (London), ser. A, vol. 194, no. 1036, July 1948, pp. 16-42.

10. Schaaf, S. A., Hurlbut, F. C., and Talbot, L.: Induced Pressures on Flat Plates in Hypersonic Low Density Flow. TR 57-47, Bell Aircraft Corp., Jan. 25, 1957. (Contract AF-18(600)-1607.)

11. Rayle, Roy E., Jr.: An Investigation of the Influence of Orifice Geometry on Static Pressure Measurements. MS Thesis, M.I.T., 1949.

12. Loeb, Leonard B.: The Kinetic Theory of Gases. Second ed., McGraw-Hill Book Co., Inc., 1934.

13. Lees, Lester, and Probstein, Ronald F.: Hypersonic Viscous Flow over a Flat Plate. Rep. No. 195, Aero. Eng. Lab., Princeton Univ., Apr. 20, 1952. (USAF Contract AF 33(038)-250.)

14. Lees, L.: Hypersonic Flow. Proc. Fifth Int. Aero. Conf., Inst. Aero. Sci., Roy. Aero. Soc. (Los Angeles), June 20-23, 1955, pp. 241-276. (See also GALCIT Pub. No. 404.)

15. Lees, L.: Note on the Hypersonic Similarity Law for an Unyawed Cone. Jour. Aero. Sci., vol. 18, no. 10, Oct. 1951, pp. 700-702.

16. Probstein, Ronald F., and Bray, Kenneth N. C.: Hypersonic Similarity and the Tangent-Cone Approximation for Unyawed Bodies of Revolution. Jour. Aero. Sci., vol. 22, no. 1, Jan. 1955, pp. 66-68.

17. Anon.: Tables of Supersonic Flow Around Cones. Tech. Rep. No. 1, Dept. Elec. Eng., M.I.T., 1947.

18. Monaghan, R. J.: An Approximate Solution of the Compressible Laminar Boundary Layer on a Flat Plate. R.&M. No. 2760, British ARC, 1953.

19. Bromley, L. A., and Wilke, C. R.: Viscosity Behavior of Gases. Ind. and Eng. Chem., vol. 43, no. 7, July 1951, pp. 1641-1648.

20. Howarth, L., ed.: Modern Developments in Fluid Dynamics; High Speed Flow. Vol. 1. Clarendon Press (London), 1953, p. 382.

21. von Kármán, Th.: The Problem of Resistance in Compressible Fluids. Reale Accad. d'Italia (Rome), Sept.-Oct. 1935, pp. 210-271.

22. Ehret, D. M.: Accuracy of Approximate Methods for Predicting Pressures on Pointed Nonlifting Bodies of Revolution in Supersonic Flow. NACA TN 2764, 1952.

23. Kendall, James M., Jr.: An Experimental Investigation of Leading-Edge Shock-Wave - Boundary-Layer Interaction at Mach 5.8. Jour. Aero. Sci., vol. 24, no. 1, Jan. 1957, pp. 47-56.

24. Probstein, Ronald F., and Elliott, David: The Transverse Curvature Effect in Compressible Axially Symmetric Laminar Boundary-Layer Flow. Jour. Aero. Sci., vol. 23, no. 3, Mar. 1956, pp. 208-224.

25. Probstein, Ronald F.: Interacting Hypersonic Laminar Boundary Layer Flow Over a Cone. Div. Eng., Brown Univ., Providence (R. I.), Mar. 1955. (Contract AF-33(616)-2798.)

26. Van Dyke, Milton D.: A Study of Hypersonic Small-Disturbance Theory. NACA Rep. 1194, 1954. (Supersedes NACA TN 3173.)

27. Hill, J. A. F., Baron, J. R., and Schindel, L. H.: Mach-Number Measurements in High-Speed Wind Tunnels. AFOSR Tech. Rep. 56-7, Naval Supersonic Lab. Rep. 145, M.I.T., Jan. 1956. (AD 81540.)

28. Blumer, C. B., Bradfield, Walter S., and Scott, C. J.: The Effect of Cone Tip Blunting on the Supersonic Conical Laminar Boundary Layer. Eng. Memo. 29, Univ. of Minn., Mar. 1954. (Contract AF-18(600)-384.)

TABLE I. - FLOW CONDITIONS OF TESTS

[Stagnation temperature, 300° K.]

Mach number, M_1	Static pressure, p_1, microns Hg	Reynolds number per inch, Re_1	Pressure ratio, p_c/p_1 (a)
3.70	49.8	880	1.106
3.91	73.0	1,510	1.114
3.97	85.1	1,860	1.117
4.05	108.8	2,540	1.120
5.47	66.5	4,530	1.207
5.73	113.3	8,980	1.223

[a]Cone semivertex angle θ_c, 3.03°.

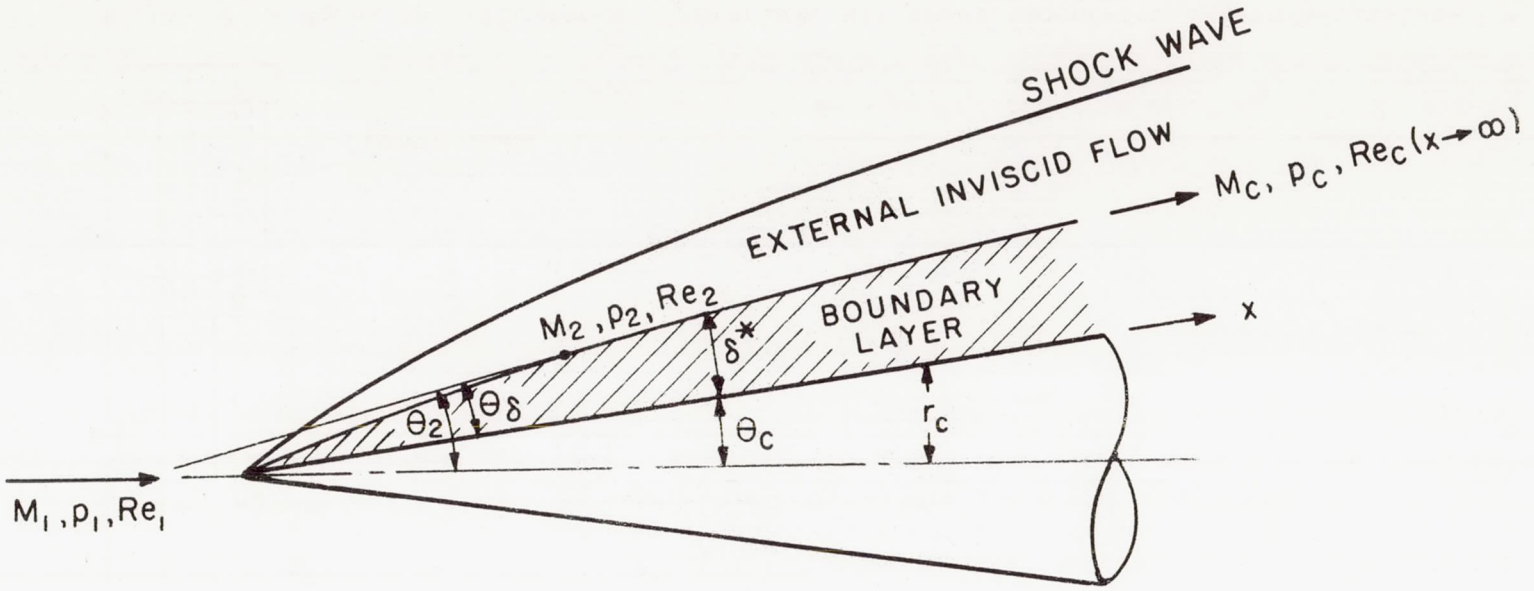

Figure 1. - Schematic drawing of viscous flow over cone.

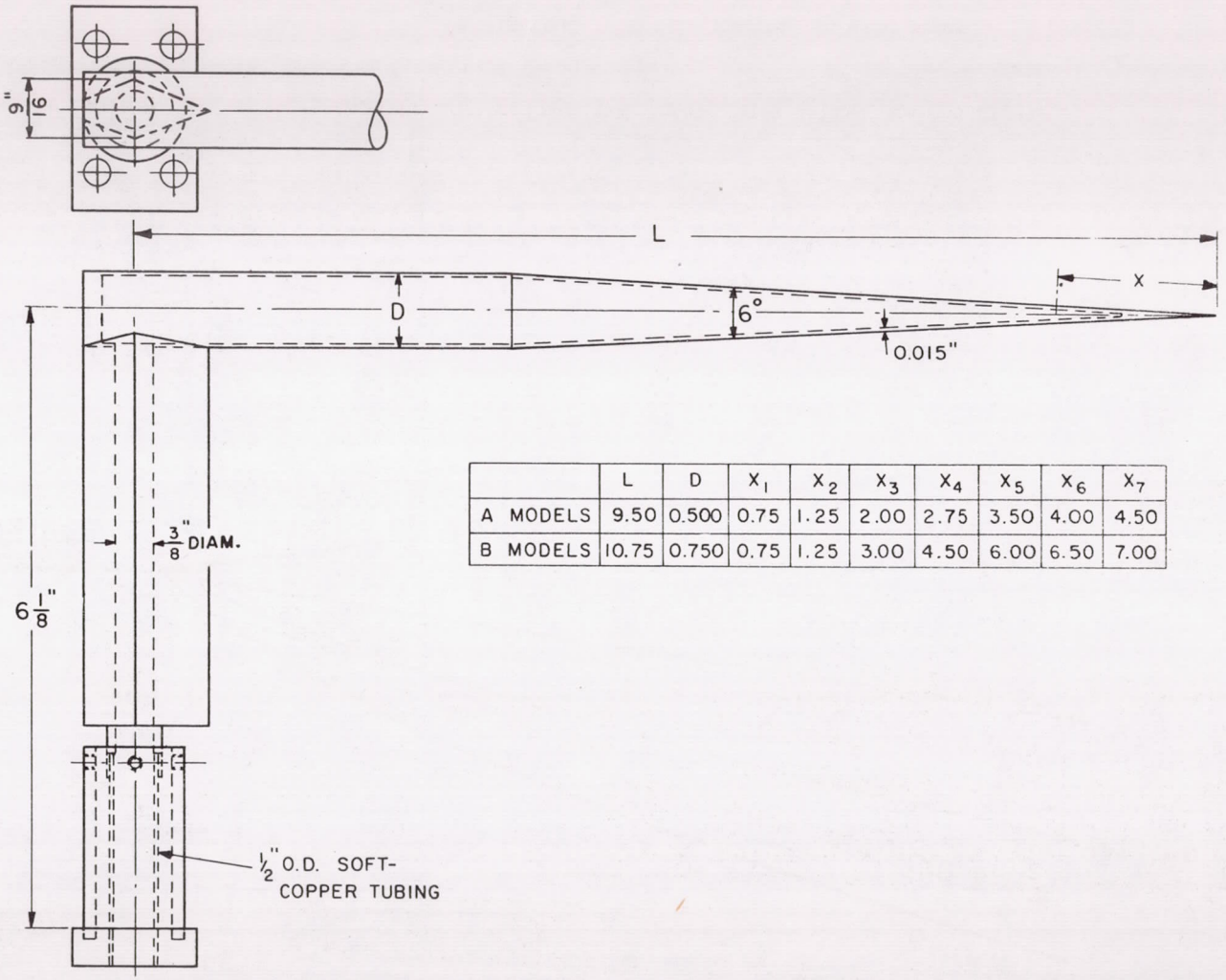

	L	D	X_1	X_2	X_3	X_4	X_5	X_6	X_7
A MODELS	9.50	0.500	0.75	1.25	2.00	2.75	3.50	4.00	4.50
B MODELS	10.75	0.750	0.75	1.25	3.00	4.50	6.00	6.50	7.00

Figure 2. - Model specifications. Material, all brass except for 1/2-inch-outside-diameter soft-copper tube; four static-pressure orifices 0.010 inch in diameter located at 90° intervals on each model at distances given in table (dimensions in inches).

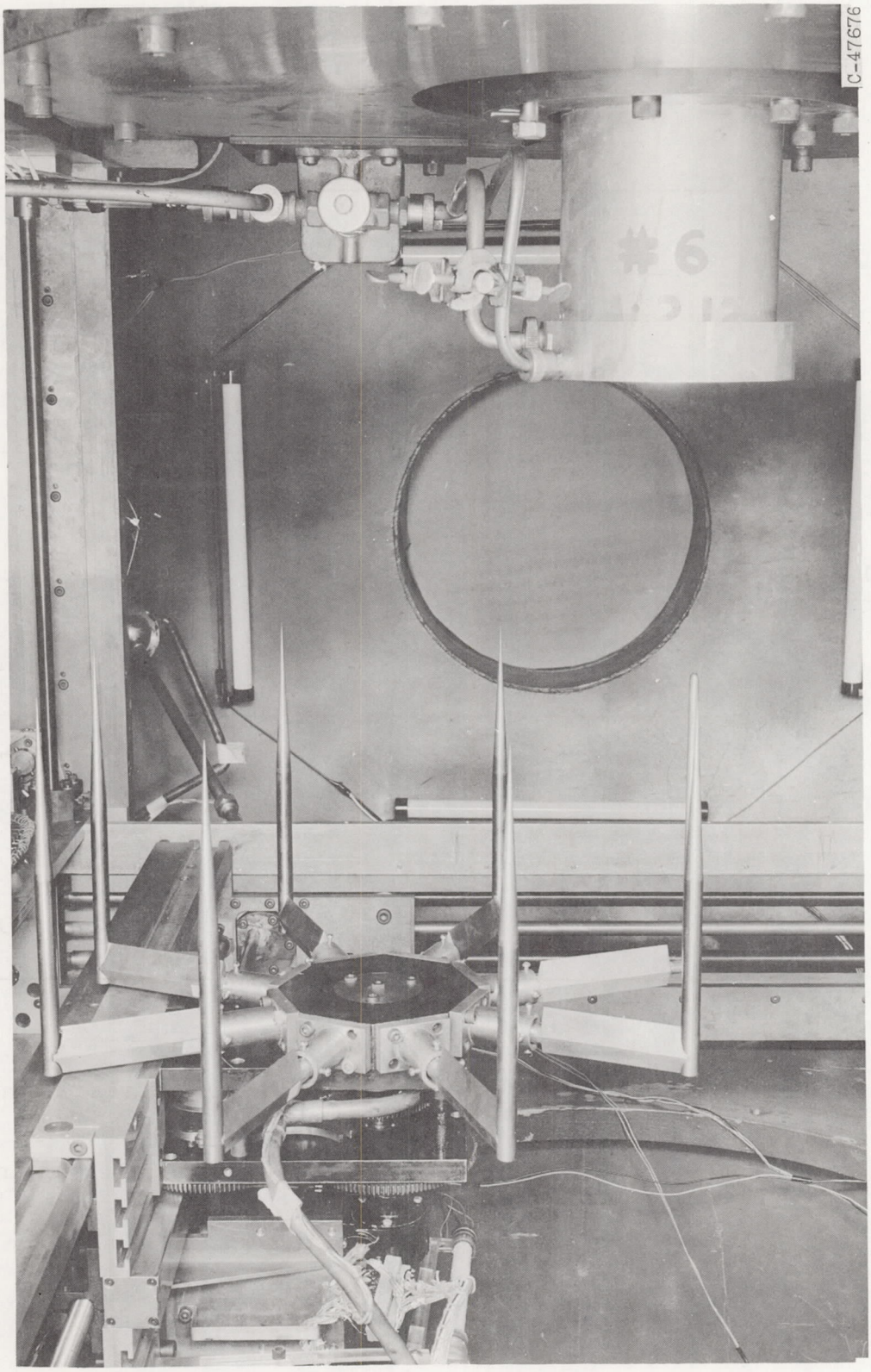

Figure 3. - Models mounted in wind tunnel.

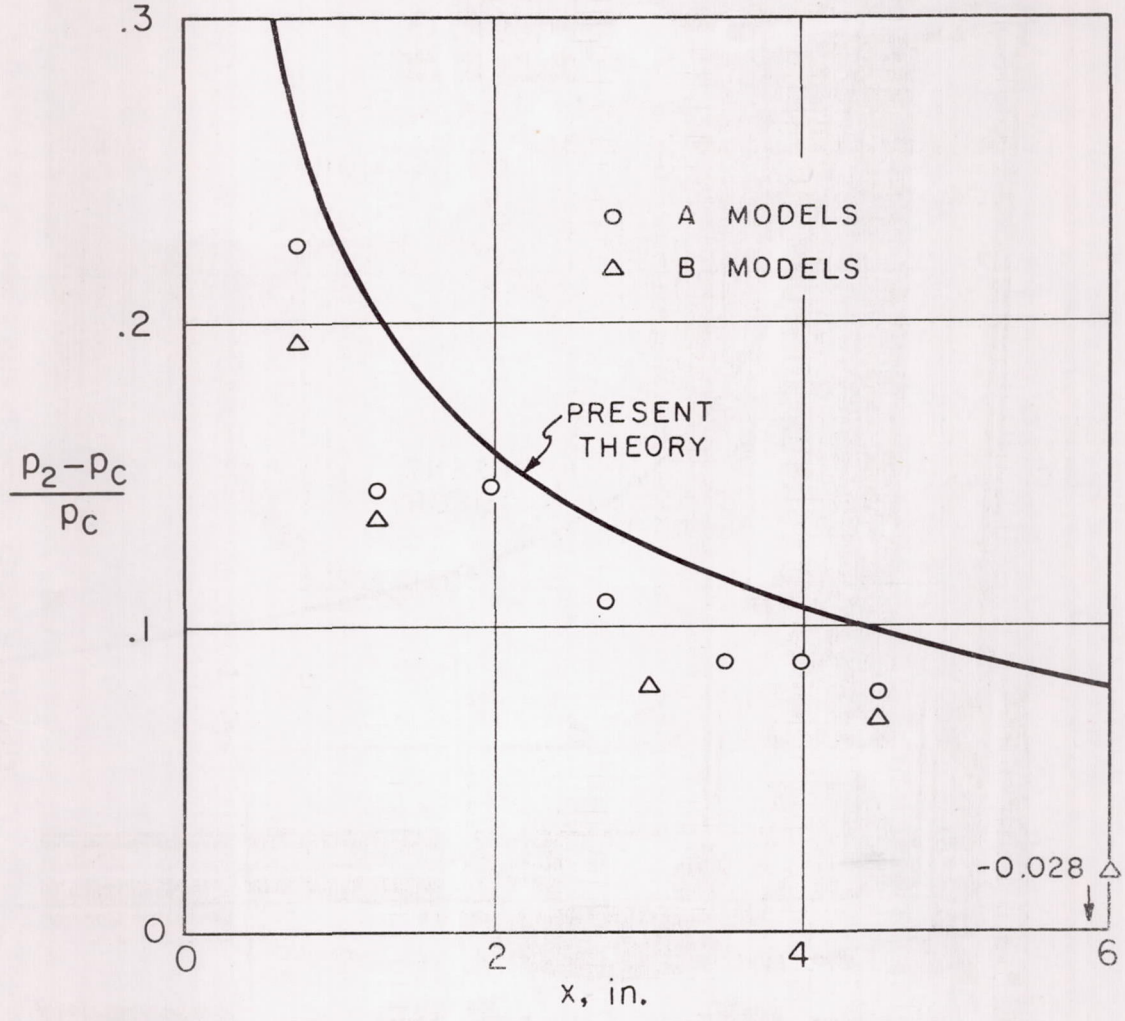

(a) Free-stream Mach number, 3.70; free-stream Reynolds number per inch, 880.

Figure 4. - Induced-pressure increment plotted against x. Cone semivertex angle, 3°.

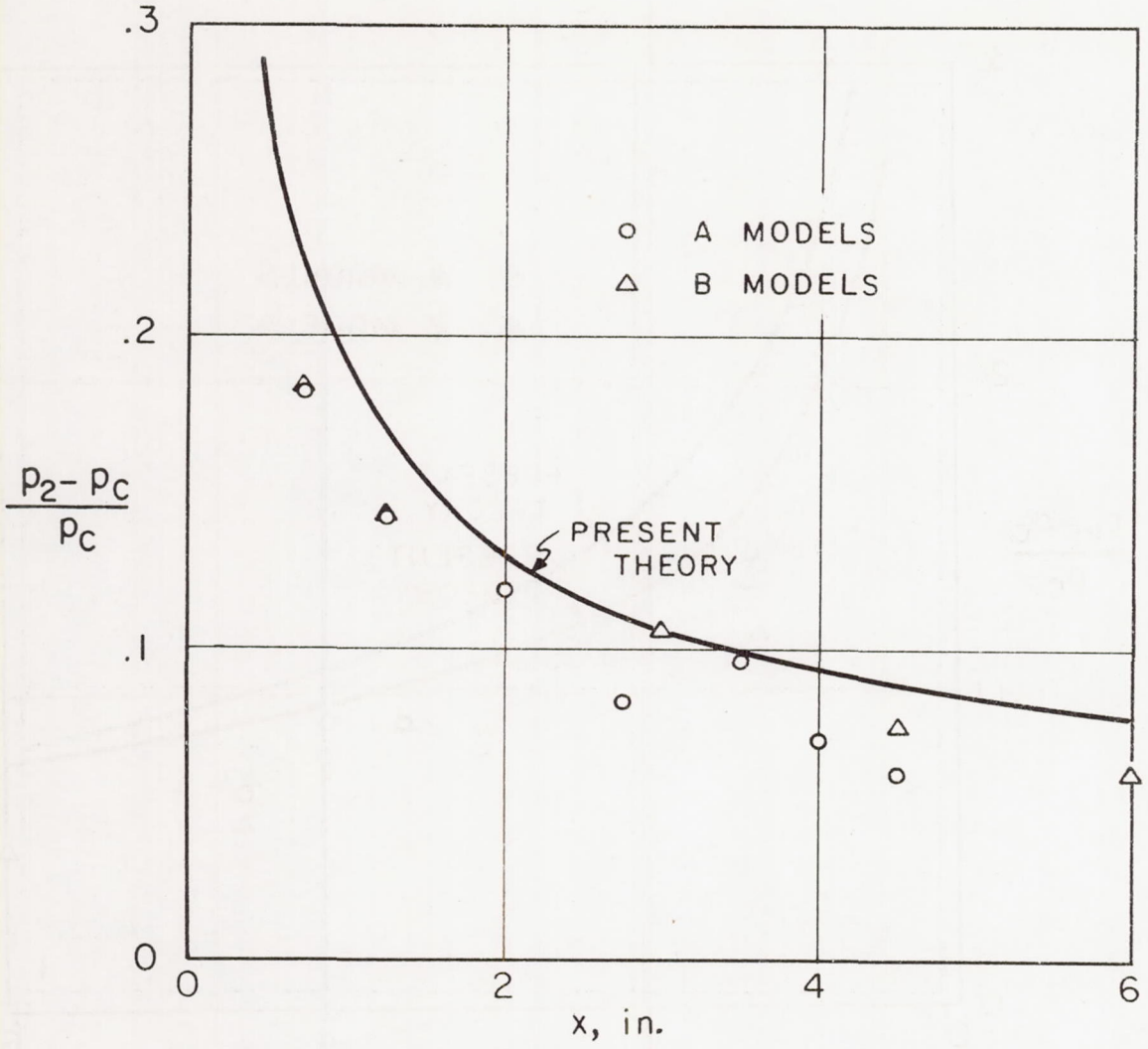

(b) Free-stream Mach number, 3.91; free-stream Reynolds number per inch, 1,510.

Figure 4. - Continued.

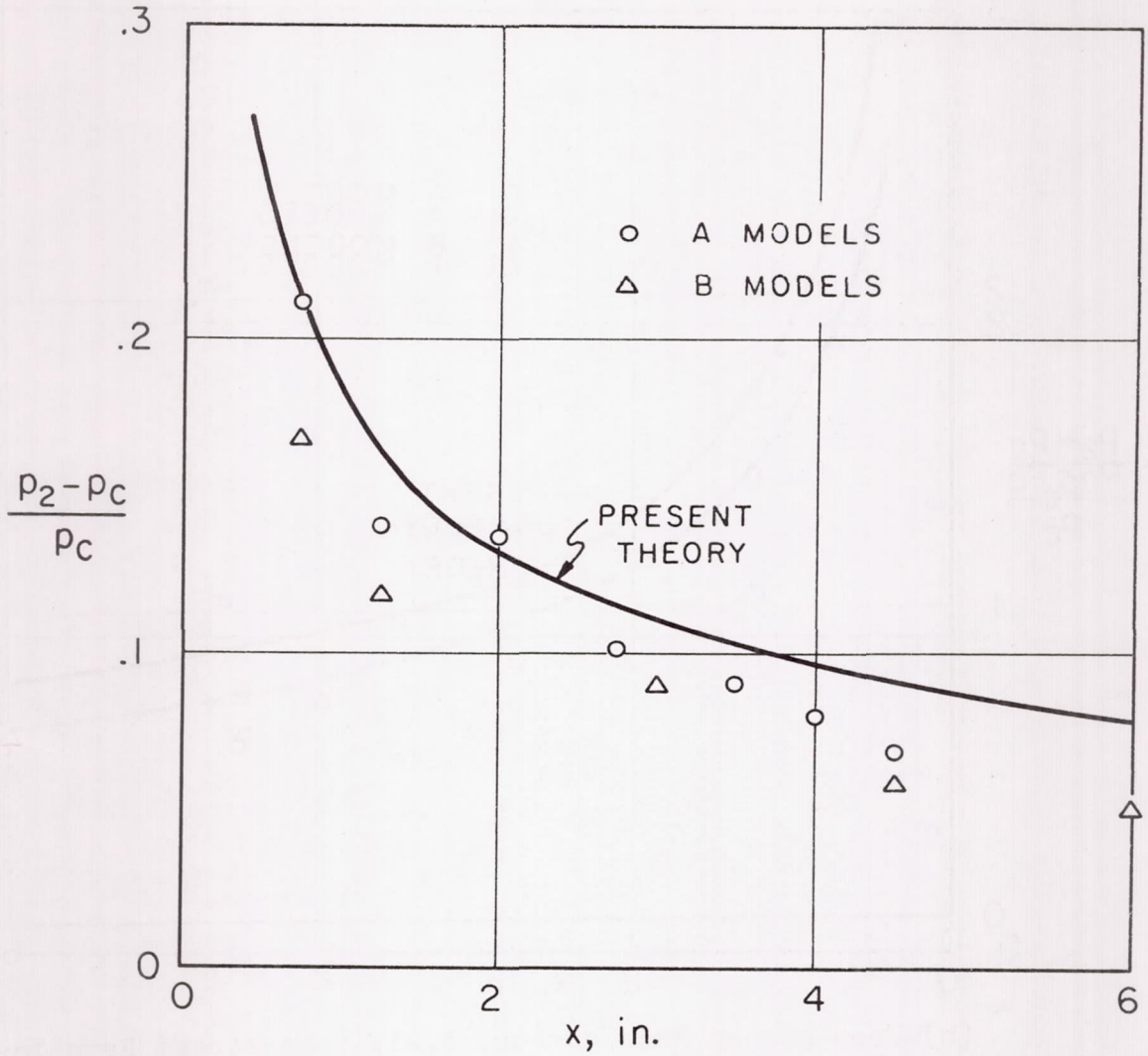

(c) Free-stream Mach number, 3.97; free-stream Reynolds number per inch, 1,850.

Figure 4. - Continued.

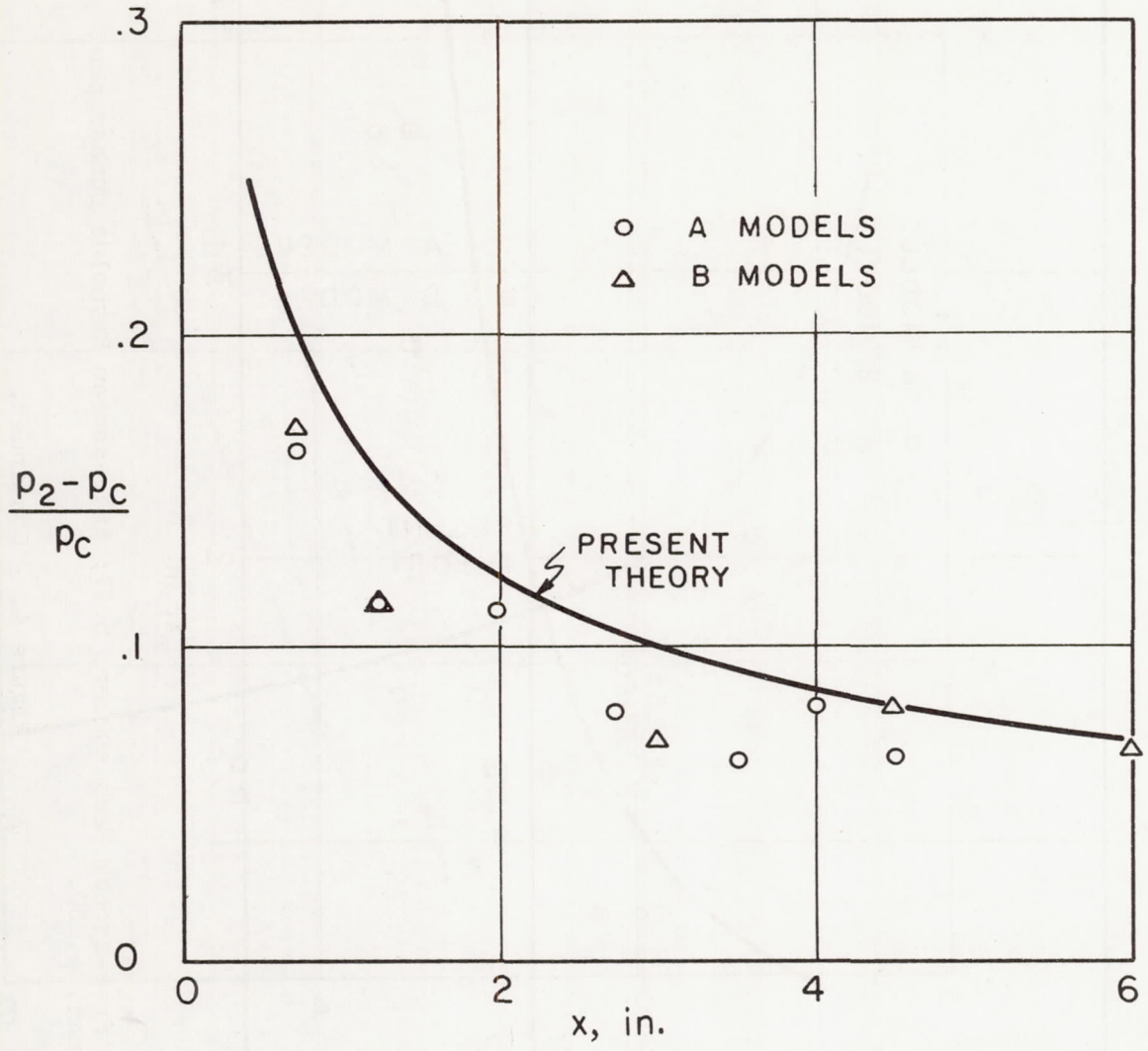

(d) Free-stream Mach number, 4.05; free-stream Reynolds number per inch, 2,540.

Figure 4. - Continued.

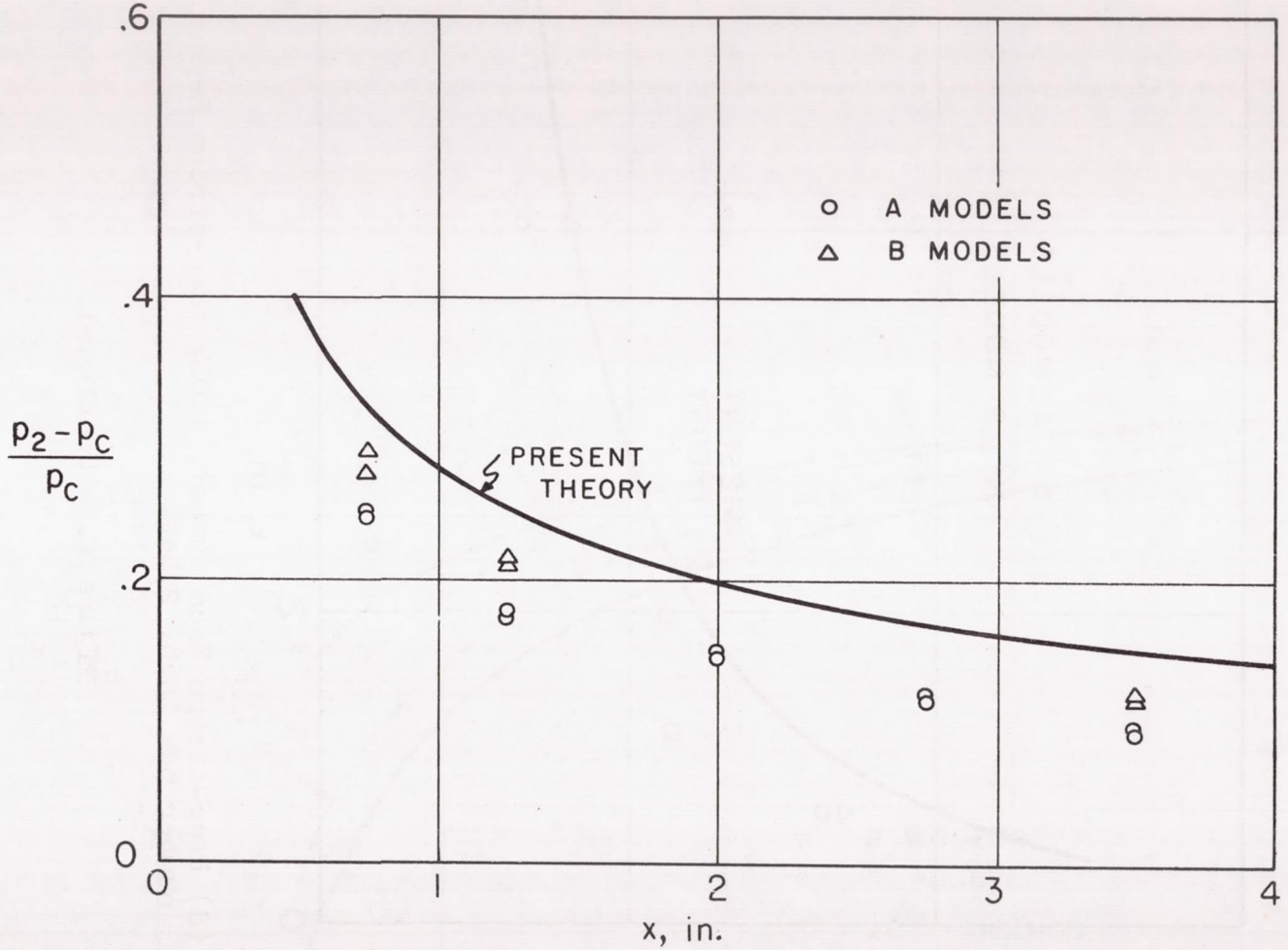

(e) Free-stream Mach number, 5.47; free-stream Reynolds number per inch, 4,530.

Figure 4. - Continued.

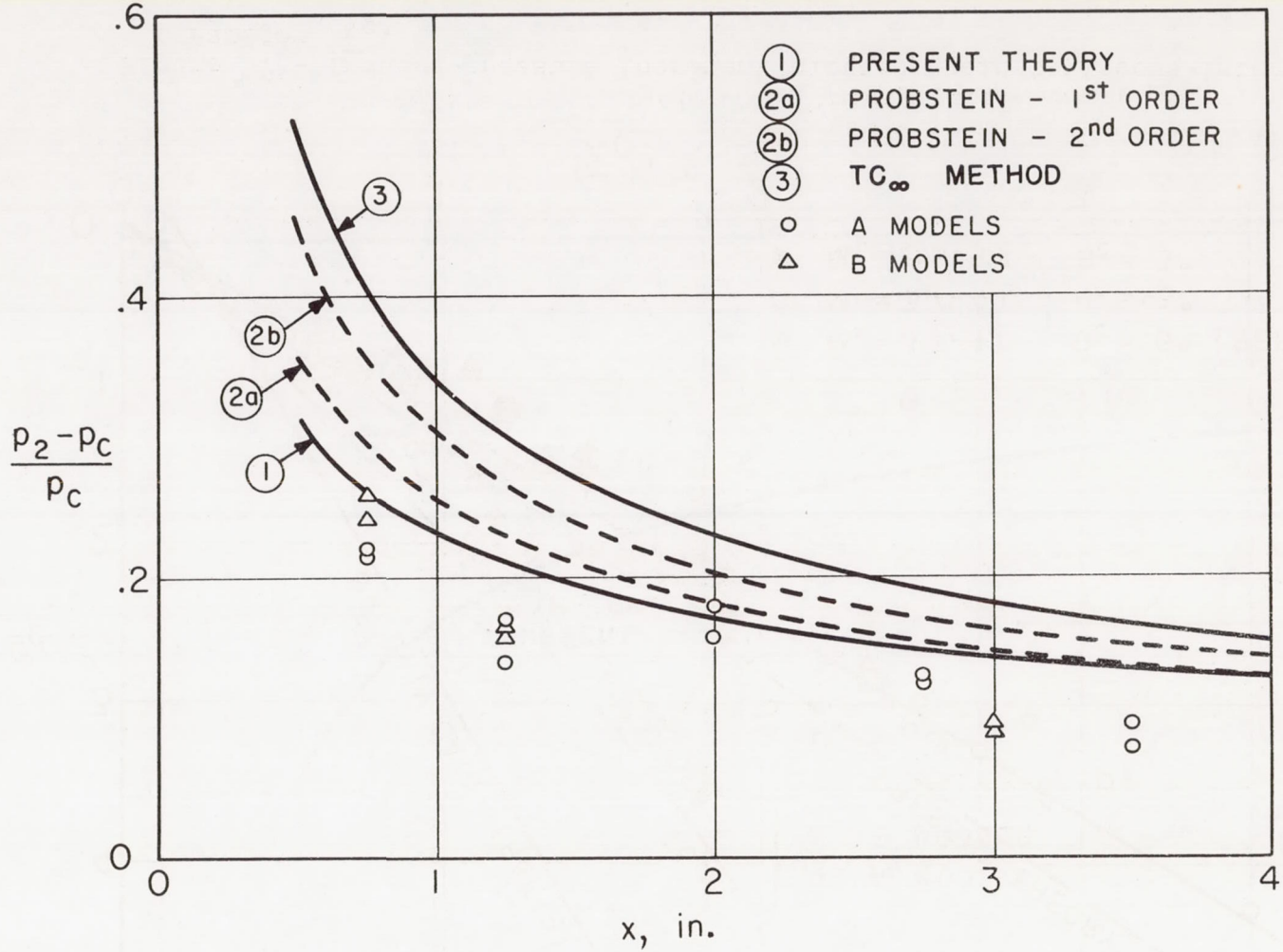

(f) Free-stream Mach number, 5.73; free-stream Reynolds number per inch, 8,980.

Figure 4. - Concluded.

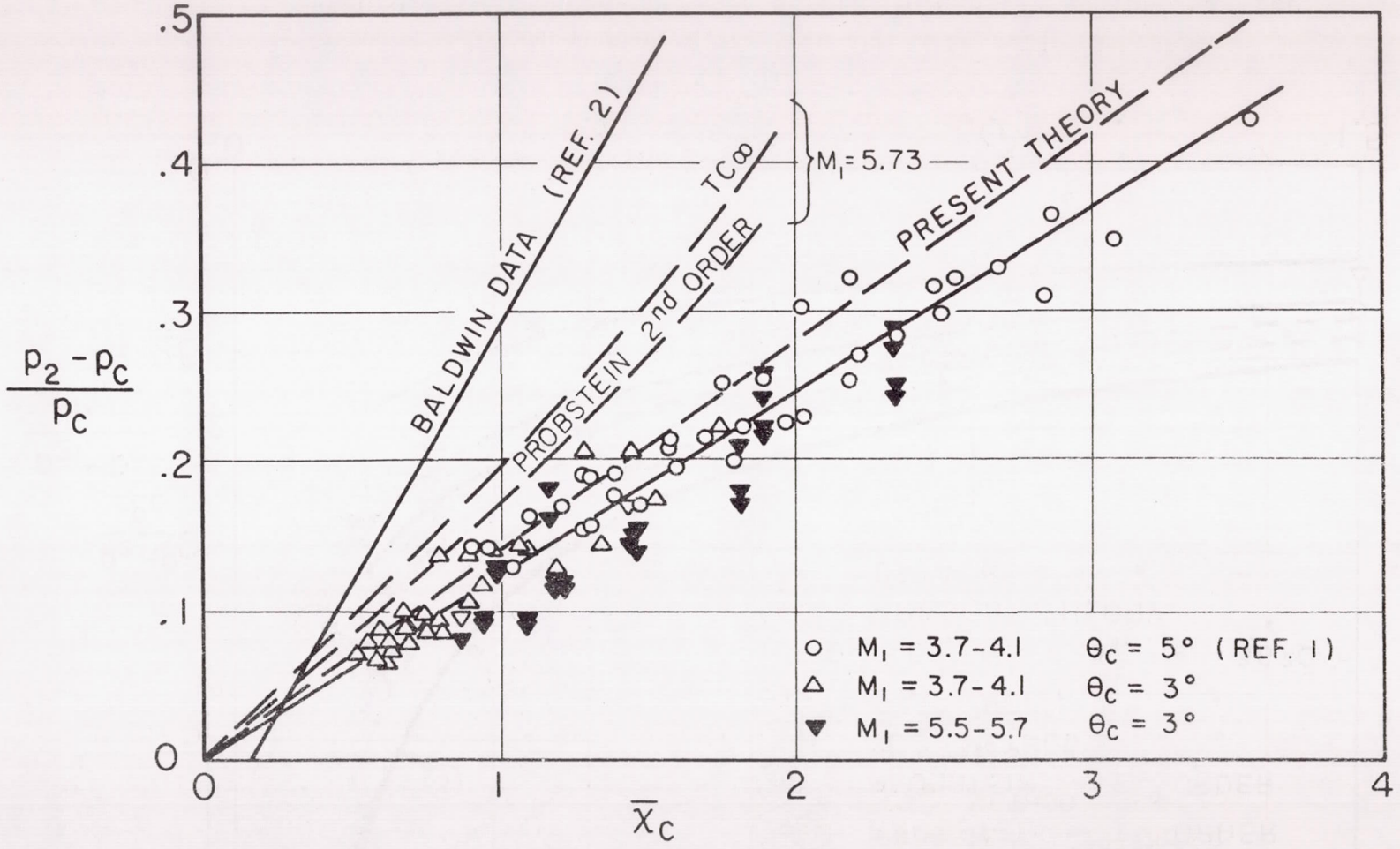

Figure 5. - Induced-pressure increment plotted against viscous-interaction parameter $\overline{\chi}_c$.

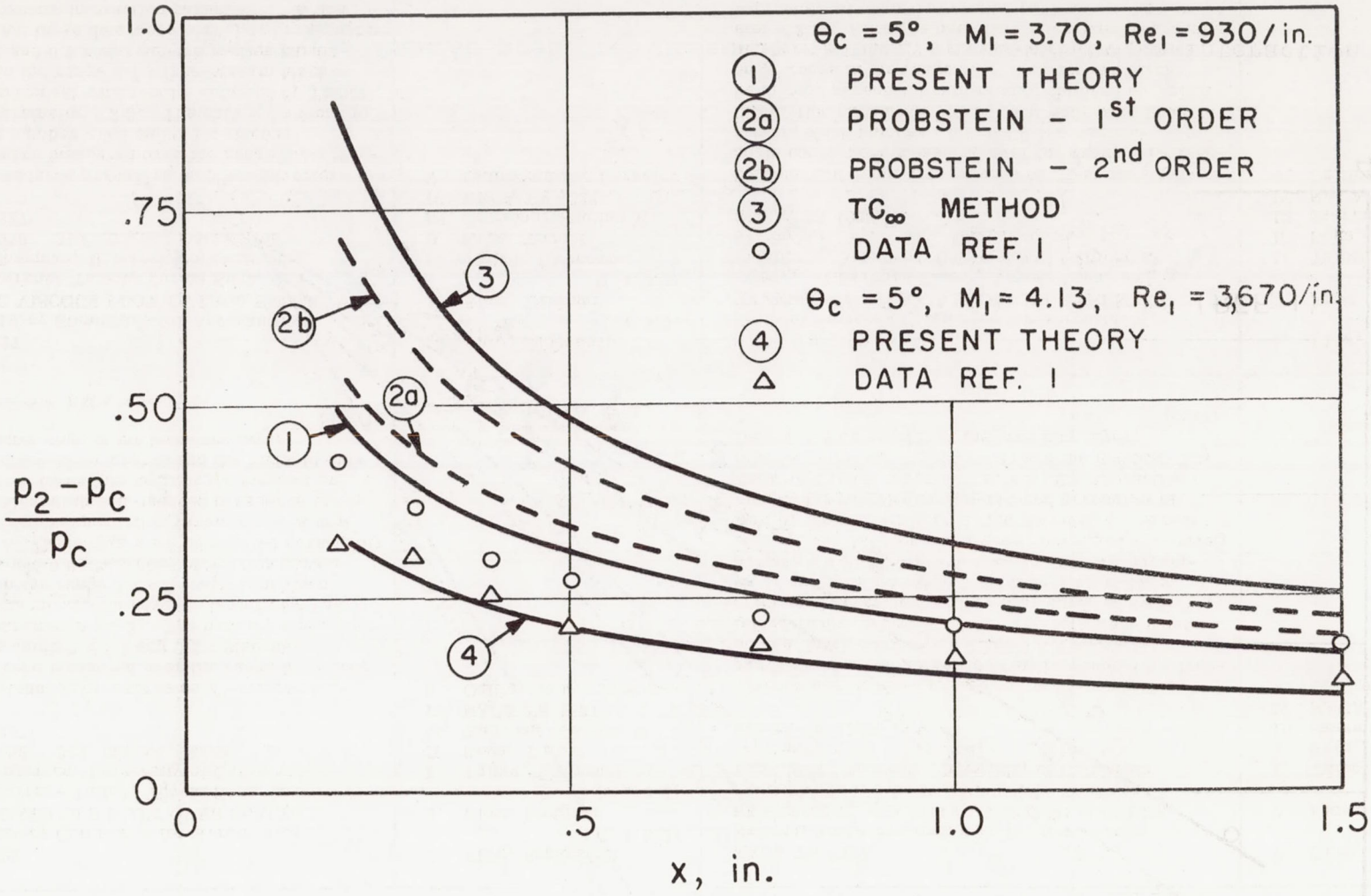

Figure 6. - Induced-pressure increment plotted against x for present data and data of reference 1.